communications earth & environment

Article

https://doi.org/10.1038/s43247-024-01724-w

# Sources of lead in a Tibetan glacier since the Stone Age

Check for updates

M. Roxana Sierra-Hernández [1] ✉, Franco Marcantonio[2], Elizabeth M. Griffith [3] & Lonnie G. Thompson [1,3]

The Tibetan Plateau glaciers, among the world's most remote and pristine places, provide water to millions and play a vital environmental role. We measured the lead isotopic composition in a dusty ice core from the Guliya ice cap in northwest Tibet, from approximately 36 thousand years Before Present (Stone Age) to 2015, to determine the onset and sources of anthropogenic lead. Despite the dust-laden nature of the core, a clear change in the lead isotope signature to below Stone Age levels started in 1949 followed by a rapid decrease in 1960 and an even more rapid decrease in 1974 indicating the first emergence of anthropogenic lead. Accurate isotopic lead measurements allowed us to better, and more sensitively, quantify sources using a Bayesian mixing model. Chinese gasoline was the primary anthropogenic source surpassing natural contributions in the 2000s until 2007 when emissions from leaded gasoline decreased and those from coal and lead-zinc ores increased.

Lead (Pb) is a toxic heavy metal ubiquitous in Earth's critical zone. It enters the human body by ingestion of Pb-contaminated water, food, soil, and inhalation of Pb-containing particles. Exposure to lead can adversely affect children's development and behavior, even at low levels, and in adults, it is associated with a number of health problems including cardiovascular effects, nerve disorders, decreased kidney function, fertility issues, and cancer[1–6].

The natural geochemical cycle of Pb has been altered since ~7000 BC by early civilizations. The oldest Pb archeological artifacts found date back to ~6400 BC[7,8] and ~5000 BC[9] suggesting that Pb has been used since the Neolithic period, before the Copper and Bronze Ages (~3300 BC-1200 BC in Europe and ~3000 BC in China). In China, archeological evidence shows that Pb was smelted during the Shang (1766-1112 BC) and the Zhou (1027-221 BC) Dynasties[10–13].

Even though Pb has been used by ancient civilizations for millennia, it was not until the Industrial Revolution and later, when leaded gasoline was introduced in Europe and North America in the 1920s, that the emission of Pb from human activities skyrocketed. By the 1980s, emissions surpassed their natural and pre-Industrial contribution by about two orders of magnitude[14,15]. Anthropogenic emissions of Pb have decreased in North America and Europe after the phase out of leaded gasoline due to proven and serious health impacts[16–18]. However, in Asia, and particularly in China, anthropogenic emissions of Pb continue to overwhelm their pre-Industrial levels[17,19,20].

Recently, a continuous and high-resolution history of trace elements (TE) including Pb between ~1650 and 2015 was reconstructed using two ice cores from the Guliya ice cap[21,22]. The Guliya ice cap, located in the northwestern Tibetan Plateau (TP), China (Fig. 1), is one of the largest ice caps in the subtropical zone (>376 $km^2$) and was drilled in 1992 and 2015[23,24]. The TP is one of the most remote places in the world and is considered to be a pristine place due to the very low industrial activity in the region[25]. In fact, it is the region with the lowest emissions of toxic metals including Pb[26]. However, two distinct periods of non-crustal, i.e., anthropogenic, deposition of Pb and other TEs such as Sn, Sb, Cd, and Zn were detected in the Guliya ice cores: ~1850–1950, and ~1970–2015[21,22].

To determine the potential sources of TEs in the Guliya ice cores, their temporal trends were compared with those of other natural archives, with emission inventories from different countries and regions, and using back trajectories to estimate the geographical areas of the air parcels reaching the Guliya ice cap[22]. Given that North America and Europe were the major anthropogenic sources of atmospheric Pb during the late 1800s and the first half of the 20$^{th}$ century, it was determined that coal combustion in western Europe was the likely source of anthropogenic Pb between 1850-1950. However, questions remained about this conclusion due to low back trajectory frequencies (<5%) and low and sporadic increases before the 1950s. Furthermore, determining post-1970s anthropogenic sources was challenging given the global increase in the number of anthropogenic emission sources. It was suggested that the metal enrichments detected in Guliya originated primarily from regional fossil fuel combustion and biomass burning and secondarily from industrial processes and agricultural activities[21]. To help shed light on the Pb sources at Guliya, and to more

[1]Byrd Polar and Climate Research Center, The Ohio State University, 108 Scott Hall, 1090 Carmack Road, Columbus, OH, 43210, USA. [2]Department of Geology and Geophysics, Texas A&M University, 3115 TAMU College Station, College Station, TX, 77843-3115, USA. [3]School of Earth Sciences, The Ohio State University, 275 Mendenhall Laboratory, 125 South Oval Mall, Columbus, OH, 43210, USA. ✉e-mail: sierra-hernandez.1@osu.edu

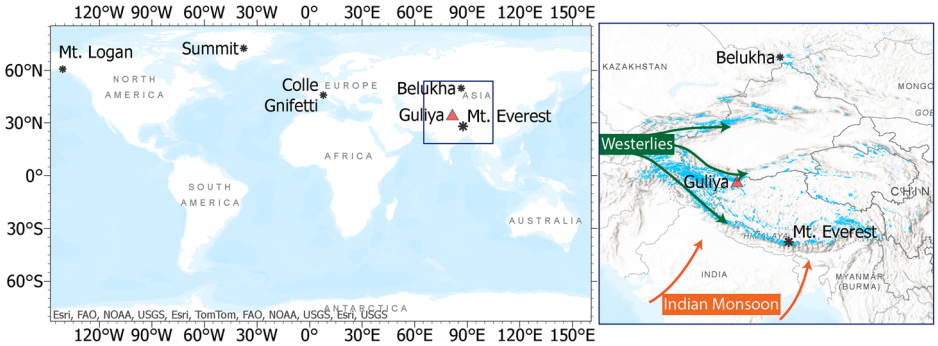


**Fig. 1 | Maps showing the locations of the Guliya ice core and other ice cores mentioned in the text.** Left map: World map showing the locations of the Guliya drilling site (red triangle) in the western Kunlun Mountains and the location of other ice cores discussed in the text. Right map: Relief map of the Tibetan Plateau (TP) illustrating the movement of the main air masses (westerlies and the summer Indian Monsoon) that influence the region. Glaciers on the TP (right map) are shown in blue.

sensitively deconvolve the various anthropogenic sources of Pb, we use Pb isotopes in this new study to track the variability of Pb sources before and after the Industrial Revolution. We present the Pb isotopic composition ($^{204}$Pb, $^{206}$Pb, $^{207}$Pb, and $^{208}$Pb) of 89 discrete samples that were used for the Guliya TE records.

Additionally, we analyzed six new samples from the Paleolithic period, the earliest period of the Stone Age, that predates the Chinese Bronze Age, to establish the natural Pb isotopic background in the region. Recent changes can then be assessed by comparison to this natural background. However, establishing a natural background of Pb is challenging as Pb has been used since the Neolithic or New Stone Age, which predates both the Copper and Bronze Ages[7–9,17]. Furthermore, the onset and degree of Pb pollution in the environment in the Northern Hemisphere show considerable temporal and spatial variation, as recorded in different natural archives[17,22]. For instance, Pb contamination appears for the first time at ~6500 BC in a sediment core from North America[17,27], while in eastern central China it appears at ~3000 BC in a lake sediment core, which suggests a more recent time for the onset of the Bronze Age in ancient China[28]. Additional ice core samples from the 1500s, and 17 potential source area (PSA) dust samples collected in the vicinity of the Guliya ice core drilling sites and around the TP are presented in this study to identify local natural Pb sources. The measurement of the low-abundance (1.4%) isotope $^{204}$Pb in this study provides valuable and highly sensitive insights into source apportionment. Most studies of Pb isotopes in ice cores are limited to analyzing only the higher-abundance isotopes of Pb ($^{206}$Pb, $^{207}$Pb, and $^{208}$Pb).

## Results and discussion

### Pb isotopic characterization of the guliya ice core samples

A changepoint detection analysis of the Pb isotope ratios (Supplementary Fig. S1) suggests a change in natural sources that started between 1689 ($^{208}$Pb/$^{207}$Pb) and 1748 ($^{207}$Pb/$^{204}$Pb, $^{208}$Pb/$^{204}$Pb) when Pb isotope ratios became slightly more radiogenic until 1919. This analysis also detected a slight decrease (less radiogenic) of the Pb isotope ratios below the Stone Age background starting in 1949 ($^{207}$Pb/$^{204}$Pb, $^{208}$Pb/$^{204}$Pb), followed by a rapid decrease in 1960 ($^{208}$Pb/$^{207}$Pb) and even a more rapid decrease after 1974 ($^{206}$Pb/$^{204}$Pb, $^{206}$Pb/$^{207}$Pb) (Fig. 2, Supplementary Figs. S1, S2). The latter changes coincide with enrichments of Pb, Sn, Cd, Zn, and to a lesser extent Sb detected in the high-resolution record (Fig. 2) previously published[21,22]. This rapid change in Pb isotopic ratios was also observed in the Everest Pb isotopic ice core record[29] around the same time. Likewise, on the other side of the world, an ice core record from Mt. Logan in the Yukon Territory, Canada, shows a sharp increase of Pb concentration in 1970 which was attributed to Pb air pollution from Asia[30] (Fig. 3).

An unsupervised machine learning method, k-means clustering, classified the ice core samples into three clusters (Supplementary Text S1, Supplementary Fig. S3). Cluster 1 comprises all pre-Bronze Age samples from the Plateau (4 samples) and the Summit (2 samples), all samples between ~1500 to 1974, and 21 post-1974 samples. Cluster 2 is formed only by post-1974 samples (31 samples) including most of the 21$^{st}$ century samples (17 samples) analyzed here. Cluster 3 is comprised of only one sample with its duplicate analysis (post-1974) that is much more radiogenic than the rest of the samples with $^{206}$Pb/$^{204}$Pb, $^{207}$Pb/$^{204}$Pb and $^{208}$Pb/$^{204}$Pb isotope ratios of 19.978, 15.726, and 38.578, respectively. The high Pb isotope ratios in this one sample could be the result of: 1) contamination during sample preparation, 2) dust originating from a different source compared to the rest of the samples, or 3) preferential dissolution of radiogenic Pb[31]. Since we cannot determine the source of this singular highly radiogenic sample, we exclude it from further discussion and focus on the samples in Clusters 1 and 2.

The main difference between the two ice core sample clusters is that Cluster 1 has a more radiogenic average Pb isotope ratio than Cluster 2. Additionally, Cluster 1 samples exhibit an average Pb EF of 1.0 while Cluster 2 samples show a value of 1.5 (Table 1). These results suggest a solely natural origin for Cluster 1 samples and an additional anthropogenic contribution for Cluster 2 samples.

Analyzing ice core samples predating the Bronze Age was important to establish a baseline of Pb isotope ratios close to the natural background before the use of Pb by ancient civilizations. The Pb isotope ratios of the samples covering the period 1500 to 1949 are similar to the Pb isotope ratios of the samples from the pre-Bronze age (Supplementary Figs. S2, S4), which provide a long-term average signal as time is more compressed in the deeper sections of the Guliya ice core. This is confirmed with the k-means cluster analysis which grouped together all the samples from before ~1974 (Cluster 1), including those from the pre-Bronze Age. Thus, Pb used by ancient civilizations is not detected in the Guliya ice core.

### Natural sources of Pb in Guliya

The Guliya ice cores are characterized by very high dust concentrations compared to other ice cores in the TP[22,24]. Dust concentrations vary considerably ($4.5 \times 10^4$ to $1 \times 10^8$ particles/ml in GP1992) due to the changes in frequency and/or intensity of dust storms in the region. The Pb concentrations of the samples for this study range between ~0.3 ng/g and ~11 ng/g with a median of ~1 ng/g[21,22]. The non-parametric Wilcoxon rank-sum test indicates that Pb isotope ratios in samples of low and high dust (Pb) concentrations before ~1974 come from populations with identical distributions. Thus, Pb in the Guliya ice core originates from the same sources during low and high dust activities before ~1974.

To determine the possible natural sources of Pb in Guliya, the Pb isotope ratios of the Cluster 1 ice core samples were compared with the potential PSA groups formed (see Methods, Tables 2–3, and Supplementary Table S1) using three-isotope plots (Fig. 4). The Cluster 1 Pb isotope ratios visually overlap with the TP PSA group in all three plots strongly suggesting that the main natural sources during the last 500 years and during ancient times are local in nature and are most likely from the Tibetan Plateau. Cluster 1 ice core samples were further compared with the TP PSAs using the non-parametric Wilcoxon rank-sum test. The $p$-values of 0.9532, 0.5290, and 0.2572 for $^{206}$Pb/$^{204}$Pb, $^{207}$Pb/$^{204}$Pb, and $^{208}$Pb/$^{204}$Pb, respectively, indicate that the rank-sum test fails to reject the null hypothesis of equal medians at the 5% significance level. In other words, it is very likely that the Pb in the Cluster 1 ice core samples originates from natural dust sources in the Tibetan Plateau.

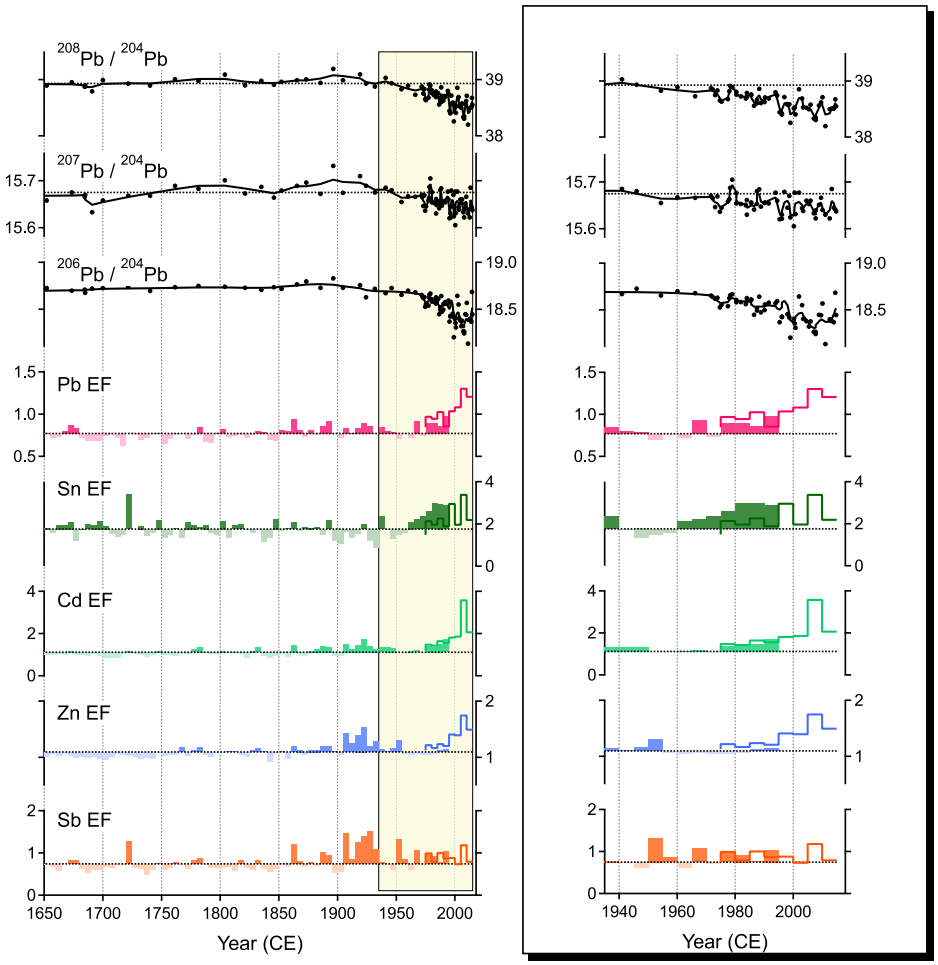


**Fig. 2 | Pb isotope ratios of the Guliya ice core (GP) samples.** The solid black lines represent the smoothed data obtained with a binomial smoothing filter for each Pb isotope ratio time series. The enrichment factor (EF) of Pb, Sn, Cd, Zn, and Sb are shown for comparison as 5-yr medians for the 1992 ice core (1650–1992) and as annual averages for the 2015 Guliya ice core (1970–2015) above and below the 350-yr (1650–1950) enrichment factor medians[21,22]. The horizontal dashed lines in the three panels for the Pb isotope ratios correspond to the respective Pb isotope ratio averaged for the two Stone Age ice core samples (36–28 Ka BP) representing the Pb isotopic signature of the natural background. The panel on the right is a "zoom–in" of the 1935–2020 period.

Other regional natural records also show relatively constant background of Pb isotope ratios dominated by mineral dust prior to the 1950–1960s. For instance, the 1205–2002 ice core record from Mt. Everest has a constant background with mean $^{206}Pb/^{207}Pb$ and $^{208}Pb/^{207}Pb$ ratios of ~1.20 and 2.50, respectively[29], which are slightly higher than the averages of 1.192 and 2.480 for Guliya. This difference is probably due to the north-south radiogenic Pb isotope gradient in Tibet (Supplementary Fig. S4) and is a function of the southerly location of Everest compared to that of Guliya (Fig. 1). Likewise, between ~1850 and ~1950, lake sediment[32] and peat bog records from Northeastern Tibet[33] were dominated by a constant natural background with mean $^{206}Pb/^{207}Pb$ ratios of 1.183 and 1.189, respectively. In contrast, the Pb isotope ratios in natural archives outside of Tibet and the Himalayas (e.g., Belukha in the Altai Mountains in Russia[34], Summit in Greenland[35], and Colle Gnifetti in the Swiss-Italian border[36], Fig. 1) show large variations prior to the 1950s (Fig. 3) as a result of local and regional anthropogenic emissions. This shows that Tibet and Himalayas remained unaffected by European/Russian anthropogenic Pb.

Two samples from the Guliya summit (GS) ice cores were analyzed to determine whether distinct sources reach the summit, located 500 m above the plateau. The cluster analysis grouped these GS samples with the GP pre-Bronze samples suggesting the GS samples are derived from similar sources. The two GS ice core samples have slightly more radiogenic Pb isotopes than the GP ice core samples of similar age (Supplementary Fig. S2). However, this is not unique as several other GP ice core samples have similar Pb isotope ratios before the 1900s. Unfortunately, with only two GS samples, other statistical tests cannot be performed. However, it appears that from ~13.5–3.5 ka BP the Pb at both the summit and the plateau originates from similar natural sources in the TP.

## Anthropogenic sources of Pb in Guliya

Cluster 2 ice core samples are less radiogenic compared to Cluster 1 and include solely post-1974 samples, strongly suggesting anthropogenic contributions. To determine the potential anthropogenic sources, we follow three approaches. First, we follow the traditional approach by comparing the Guliya ice core samples with potential anthropogenic sources using three-isotope plots. Then, we compare the temporal trends of the Guliya Pb isotope ratios with the major potential Pb emission sources. And finally, we use the Bayesian mixing model MixSIAR to quantify the contribution of the potential Pb sources.

**Three isotope plots comparison.** For the three-isotope plots, we used the following anthropogenic potential sources: coal, gasoline, and Pb/Zn ores from China[37]; coal and gasoline from UK/Europe[38–40]; Pb ores from Kazakhstan[41]; and urban aerosols collected prior to 2000 from Islamabad in Pakistan, Alma Ata in Kazakhstan, Ahmedabad in India, and Eastern China cities including Hong Kong, Xin Shao, Cheng Du and Beijing[42]. Unfortunately, published Pb isotopic ratio studies of potential anthropogenic sources seldomly include measurements of the low abundance isotope, $^{204}Pb$, as we do here. Despite this, the three-isotope plots $^{207}Pb/^{204}Pb$ vs. $^{206}Pb/^{204}Pb$, $^{208}Pb/^{204}Pb$ vs. $^{206}Pb/^{204}Pb$, and $^{208}Pb/^{207}Pb$ vs. $^{206}Pb/^{207}Pb$, are presented in Fig. 5.

Figure 5a shows that the Pb isotope ratios of the Cluster 2 ice core samples visually match best with the Chinese coal and Chinese Pb/Zn ore fingerprints. However, looking at Fig. 5b, c, it is clear that these ratios are slightly shifted toward the Chinese fuels fingerprint.

Other potential anthropogenic sources such as British and European coal and gasoline were also considered. European gasoline Pb isotope ratios are much lower than those in the Guliya Cluster 2 samples. In fact, Pb in

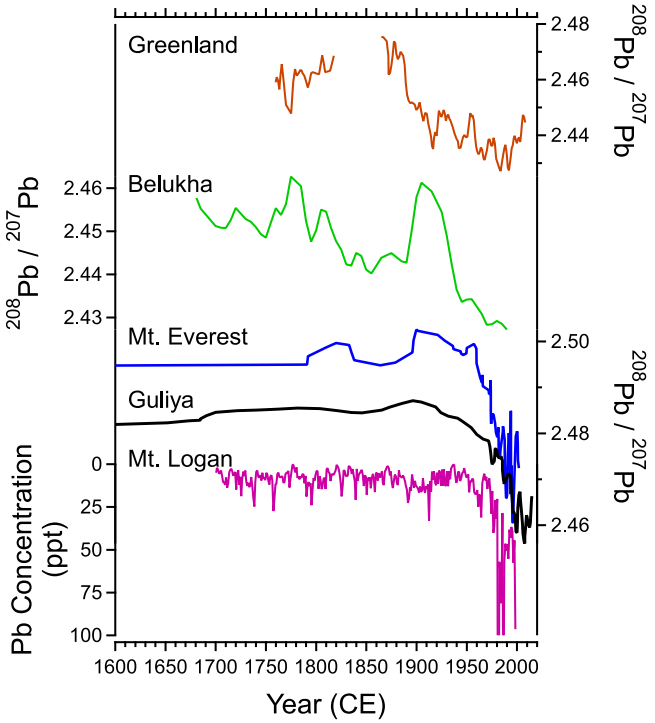


**Fig. 3 | Comparison of the $^{208}$Pb/$^{207}$Pb isotope ratios with other ice core records.** The Guliya (this study) smoothed $^{208}$Pb/$^{207}$Pb dataset (binomial smoothing filter) is compared with that of Mt. Everest in the Himalayas[29], Belukha in the Altai Mountains[34], Summit in Greenland[35], and with the Pb concentration in the Mt. Logan ice core, Yukon Territory[30]. Note that the Pb concentration for Mt. Logan is reversed.

British and European coal and gasoline have the least radiogenic isotope values with mean $^{206}$Pb/$^{204}$Pb, $^{207}$Pb/$^{204}$Pb and $^{208}$Pb/$^{204}$Pb isotope ratios of 17.076, 15.512, and 36.842, respectively. Thus, British and European gasoline is excluded as an anthropogenic source of Pb for Guliya.

As shown in Sierra-Hernández et al.[21] the Guliya ice cap is strongly influenced by air parcels from Central Asia including Pakistan and Kazakhstan during winter, and from both Central Asia and northern India during summer. To determine if Pb from these regions reached Guliya, the aerosols collected in Pakistan, Kazakhstan, and India are also shown in Fig. 5. These aerosols were collected before leaded gasoline was banned in each country, and therefore represent primarily local emissions from leaded gasoline[42]. The Pb isotope ratios of these aerosols are much less radiogenic than those from Guliya indicating that the aerosols from these cities likely did not reach Guliya.

To determine if emissions from Chinese sources (e.g., gasoline, coal) are potential sources of Pb at the Guliya ice cap, the Guliya Pb isotope ratios are compared with Chinese aerosols that were influenced by Chinese anthropogenic sources. The Pb in Chinese aerosols collected in cities in Eastern China was mostly influenced by local emissions from Chinese gasoline, Chinese ores, and Chinese coal[42]. The Pb in these aerosols (except Xin Shao, whose Pb isotope ratios are comparable to those from Guliya) is slightly less radiogenic than the Guliya Pb suggesting similar sources. This difference may result from the varying proportions of Pb contributed by different sources. Guliya is primarily influenced by dust sources, thus its Pb isotope ratios are less affected by anthropogenic sources and tend to be higher than those found in aerosols collected near anthropogenically active areas. Thus, in the subsequent sections we focus on Chinese coal, Chinese fuels, and Chinese ores as the likely potential sources of Pb at Guliya.

It is important to note that the Pb isotope ratios of Chinese coals used here originate from a comprehensive and large data set of 173 coal samples

**Table 1 | Average and standard deviation Pb concentration, Pb enrichment factor, and Pb isotope ratios for Cluster 1 and Cluster 2 of the Guliya ice core samples**

| | Cluster 1: pre-1974, Natural Background | | Cluster 2: post-1974, Anthropogenic | |
|---|---|---|---|---|
| | average | St dev | average | St dev |
| Pb (pg/g) | 1381 | 1578 | 560 | 243 |
| Pb EF | 1.0 | 0.7 | 1.5 | 1 |
| $^{206}$Pb/$^{204}$Pb | 18.684 | 0.09 | 18.395 | 0.10 |
| $^{207}$Pb/$^{204}$Pb | 15.668 | 0.02 | 15.644 | 0.02 |
| $^{208}$Pb/$^{204}$Pb | 38.864 | 0.1 | 38.506 | 0.12 |
| $^{208}$Pb/$^{206}$Pb | 2.080 | 0.009 | 2.093 | 0.01 |
| $^{207}$Pb/$^{206}$Pb | 0.839 | 0.004 | 0.851 | 0.00 |
| $^{206}$Pb/$^{207}$Pb | 1.193 | 0.005 | 1.175 | 0.01 |
| $^{208}$Pb/$^{207}$Pb | 2.480 | 0.005 | 2.461 | 0.01 |

from major coal mines across 18 provinces in China and, notably, includes measurements of $^{206}$Pb/$^{204}$Pb, $^{207}$Pb/$^{204}$Pb, and $^{208}$Pb/$^{204}$Pb[37] for all coal samples. The Pb isotopic signatures of Chinese coals show large variability (Fig. 5), overlapping with those of local natural sources within a limited area in the more radiogenic part of the range (Supplementary Fig. S5). Despite this overlap, there is a clear separation between the natural and the anthropogenic Pb isotopic signatures, which assists in the determination of sources.

**Temporal trend comparison with Pb emissions by source.** Figure 6 shows a temporal comparison of Guliya $^{206}$Pb/$^{204}$Pb isotope ratios with estimated Pb emissions from coal combustion, liquid fuel combustion (crude oil, fuel oil, kerosene, diesel, and gasoline) and non-ferrous metal smelting between 1950 and the 2000s in China[19].

The changes in the Guliya Pb isotope ratios reflect anthropogenic Pb emission changes in China. The decrease in Pb isotope ratios in Guliya began in 1960 following the establishment of China as a Republic and when the Pb emissions from gasoline began to rise in China. The decrease in Pb isotope ratios is more pronounced after 1980 when the Pb emissions from leaded gasoline rise exponentially likely reflecting increased energy demand in China in 1978 when it adopted a policy of openness and reform. These changes are also recorded in several Pb sediment records across China[20].

The Pb emissions from liquid fuels decreased in 1991 due to the introduction of low-leaded gasoline[19]. This reduction is reflected in the Guliya Pb isotope ratios, which were slightly higher at the time. However, as the number of vehicles continued to increase, so did the Pb emissions, leading to a return to lower Pb isotope ratios at Guliya between the mid-1990s to 2000 (Fig. 6a). A sharp decrease in Pb emissions from liquid fuels occurred in 2000 when leaded gasoline was phased out, resulting in another concurrent small increase in the Pb isotope ratios. However, the increase was short-lived, and Pb isotope ratios again decrease until ~2007.

In 2000, coal combustion became the largest source of Pb emissions nationwide in China. However, regional aerosol studies revealed varying primary sources of atmospheric Pb. For instance, aerosols collected in Northern and Eastern China exhibit more radiogenic Pb isotope ratios suggesting coal combustion as the main source[37]. Conversely, aerosols from Southern China showed stable Pb isotope ratios, suggesting no change in the sources. In Southwestern China, despite the ban on leaded gasoline, aerosol Pb isotope ratios continued to decrease to less radiogenic values, indicating that vehicles remained an important source of Pb, which could be attributed to either the continued use of leaded gasoline or the substantial increase in number of vehicles[37].

Likewise, the Pb isotope ratios in the Guliya ice core continue to decrease after 2000 reaching a minimum in ~2007 after which they seem to slowly increase. In the Xinjiang Province, north of Guliya, coal combustion

**Table 2 | Locations, Pb isotope ratios, standard errors (2σ), and assigned grouping for the 17 Potential Source Area dust samples measured in this study**

| PSA Site | PSA Group | Lat. | Long. | $^{206}Pb/^{204}Pb$ | Std Err | $^{207}Pb/^{204}Pb$ | Std Err | $^{208}Pb/^{204}Pb$ | Std Err |
|---|---|---|---|---|---|---|---|---|---|
| Guliya Army | TP | 37.09 | 76.97 | 18.704 | 0.002 | 15.657 | 0.001 | 38.898 | 0.003 |
| Guliya Camp | TP | 35.21 | 81.53 | 18.547 | 0.001 | 15.623 | 0.001 | 38.723 | 0.003 |
| Guliya Bottom Outlet G1 | TP | 35.21 | 81.53 | 18.643 | 0.004 | 15.652 | 0.003 | 38.801 | 0.008 |
| Guliya Middle Outlet G2 | TP | 35.21 | 81.41 | 18.620 | 0.002 | 15.657 | 0.001 | 38.785 | 0.003 |
| Guliya Top Outlet G3 | TP | 35.21 | 81.41 | 18.639 | 0.002 | 15.674 | 0.002 | 38.814 | 0.004 |
| Guliya Lake 1 | TP | 34.80 | 81.26 | 18.773 | 0.002 | 15.720 | 0.001 | 39.063 | 0.004 |
| Guliya Lake 2 | TP | 34.65 | 80.90 | 18.853 | 0.001 | 15.734 | 0.001 | 39.099 | 0.003 |
| Guliya Road | TP | 33.19 | 79.83 | 18.696 | 0.004 | 15.679 | 0.003 | 39.049 | 0.008 |
| Puruogangri | TP | 33.917 | 89.083 | 18.670 | 0.012 | 15.671 | 0.010 | 39.085 | 0.025 |
| Xining | TP | 32.44 | 95.57 | 18.712 | 0.002 | 15.651 | 0.002 | 38.911 | 0.004 |
| Huahaizi | Northeastern TP | 38.800 | 94.350 | 18.473 | 0.001 | 15.645 | 0.001 | 38.730 | 0.002 |
| Dunde | Northeastern TP | 38.100 | 96.400 | 18.622 | 0.002 | 15.649 | 0.002 | 38.818 | 0.005 |
| Quinghai | Northeastern TP | 36.617 | 101.767 | 18.614 | 0.004 | 15.624 | 0.004 | 38.814 | 0.009 |
| NMY 3 | NMY 3 | 29.325 | 87.000 | 18.687 | 0.002 | 15.681 | 0.002 | 39.077 | 0.005 |
| NMY 8 | Southwest TP | 30.121 | 83.380 | 18.855 | 0.005 | 15.744 | 0.004 | 39.345 | 0.010 |
| NMY 9 | Southwest TP | 30.621 | 82.283 | 18.862 | 0.002 | 15.732 | 0.002 | 39.266 | 0.004 |
| NMY 21 | Southwest TP | 30.50 | 81.31 | 18.981 | 0.001 | 15.785 | 0.001 | 39.461 | 0.002 |

*TP* Tibetan Plateau, *NMY* Naimona'nyi glacier.

**Table 3 | Pb isotope ratio means for each PSA group created**

| PSA Group | $^{206}Pb/^{204}Pb$ | $^{207}Pb/^{204}Pb$ | $^{208}Pb/^{204}Pb$ | $^{208}Pb/^{206}Pb$ | $^{207}Pb/^{206}Pb$ | $^{206}Pb/^{207}Pb$ | $^{208}Pb/^{207}Pb$ |
|---|---|---|---|---|---|---|---|
| Aral Sea | 18.634 | 15.642 | 39.049 | 2.0955 | 0.8398 | 1.1913 | 2.4964 |
| Eastern TP | 18.786 | 15.673 | 38.999 | 2.0759 | 0.8343 | 1.1989 | 2.4883 |
| Gobi Desert | 18.841 | 15.638 | 38.641 | 2.0477 | 0.830 | 1.2047 | 2.471 |
| NMY 3 | 18.687 | 15.681 | 39.077 | 2.0912 | 0.8391 | 1.1916 | 2.492 |
| Northeastern TP | 18.583 | 15.651 | 38.789 | 2.0874 | 0.8422 | 1.1872 | 2.4784 |
| Southwest TP | 18.900 | 15.753 | 39.357 | 2.0824 | 0.8335 | 1.1997 | 2.4985 |
| TP | 18.683 | 15.669 | 38.916 | 2.083 | 0.8387 | 1.1923 | 2.4836 |
| Taklamakan | 18.862 | 15.674 | 38.962 | 2.0657 | 0.831 | 1.2034 | 2.4857 |
| Taklamakan North | 18.658 | 15.667 | 38.837 | 2.081 | 0.8397 | 1.191 | 2.4789 |
| Thar Desert | 18.657 | 15.857 | 40.009 | 2.0353 | 0.8499 | 1.2393 | 2.5231 |

began increasing in the 1950s but in ~2007 it increased exponentially, which coincides with the change in trend of Pb isotope ratios at Guliya at this time (Fig. 6b). Thus, taken together, these temporal trends suggest that Pb from gasoline was the primary source of anthropogenic Pb at Guliya likely with contributions from coal combustion. Hence, gasoline remained the primary source of anthropogenic Pb at Guliya until 2007 even though leaded gasoline was phased out in 2000, probably as the result of the continuous use of leaded gasoline and/or the remobilization of legacy Pb[20]. After 2007, coal combustion emerged as the primary Pb source.

**MixSIAR mixing model.** To estimate the quantitative contribution of the potential natural and anthropogenic sources through time at Guliya, we used the mixing model MixSIAR[43–45].

Using $^{206}Pb/^{204}Pb$, $^{207}Pb/^{204}Pb$, and $^{208}Pb/^{204}Pb$ isotope ratios[44], the MixSIAR model was run using three natural sources located upwind from Guliya: TP PSA and Southwest TP and Taklamakan (Tables 2 and 3); and the three potential Chinese anthropogenic sources: coal, liquid fuels (gasoline and diesel), and Pb/Zn ores. The MixSIAR results are shown in Fig. 7. MixSIAR estimates contributions from all sources provided even if they are not relevant. Such contributions are, therefore, a reflection of the uncertainty in the contributions estimated by the model. This uncertainty is apparent in the model estimates of mean contributions of ~12%, 2%, and >1% from fuels, Pb/Zn ores, and coal, respectively, for the Stone Age ice core samples.

The median contribution from coal remains constant for the entire record. This might be inaccurate especially for the 2000s when coal Pb emissions surpassed those from gasoline. This can be explained as follows. To run MixSIAR, all potential sources must be included in the model including a natural source for pollution tracing[44]. The model requires the sources to be normally distributed and to follow a multivariate normal distribution for all Pb isotope ratios. Additionally, the Pb isotope ratios must be well-constrained for each source and be statistically different amongst themselves. This was an issue for our study as Chinese coals show a) large variability in the Pb isotope ratios (SI), and b) the Pb isotopic fingerprint of the TP PSA, which very likely represents the primary natural source of Guliya, overlaps with the most radiogenic part of the Chinese coals' fingerprint. Thus, the contributions from coal are probably underestimated with the MixSIAR model.

Bi et al. [37] determined that the Pb isotopic composition of Chinese fuels ranged between 17.376 and 18.461 for the $^{206}Pb/^{204}Pb$ isotope ratio, between 1.089 and 1.175 for the $^{206}Pb/^{207}Pb$ isotope ratio, and between 2.079 and 2.204 for the $^{208}Pb/^{206}Pb$ isotope ratio. While there is some similarity

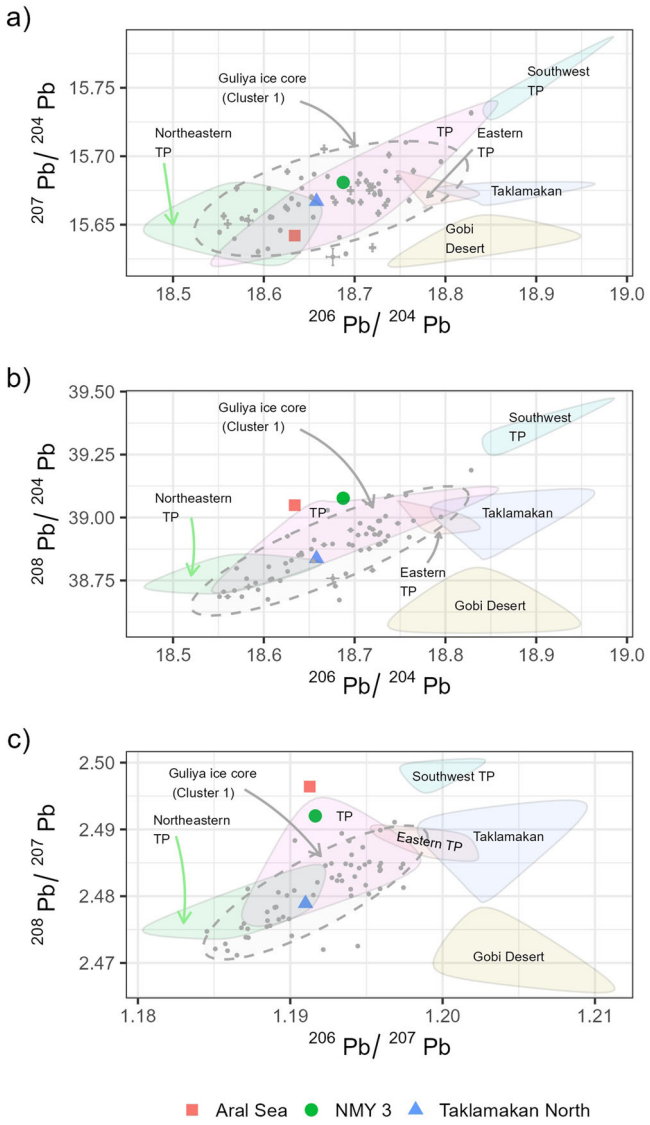


**Fig. 4 | Three-isotope plots for Guliya and natural sources.** Three-isotope plots comparing the Cluster 1 (pre-1974) ice core samples (gray circles encircled by an ellipse at 95% confidence level) with PSA groups (SI)[55–58]: **a** $^{207}Pb/^{204}Pb$ vs. $^{206}Pb/^{204}Pb$, **b** $^{208}Pb/^{204}Pb$ vs. $^{206}Pb/^{204}Pb$, and **c** $^{208}Pb/^{207}Pb$ vs. $^{206}Pb/^{207}Pb$. PSAs that were not grouped with other PSAs are depicted as discrete colored symbols. Error bars (2σ) of ice core samples are considerably smaller than the symbols in most samples. NMY: Naimona'nyi expedition/glacier; TP: Tibetan Plateau.

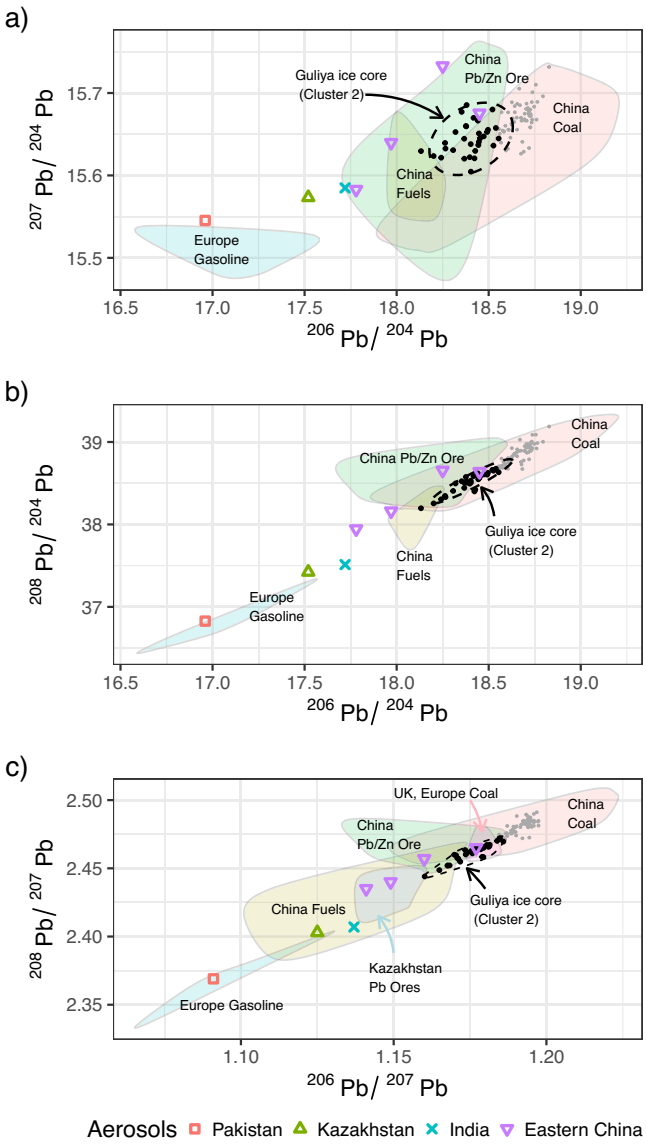


**Fig. 5 | Three-isotope plots for Guliya and anthropogenic sources.** Three-isotope plots comparing the Cluster 2 (post-1974) ice core samples (solid black circles encircled by an ellipse at 95% confidence level) with anthropogenic potential sources[37–42]: **a** $^{207}Pb/^{204}Pb$ vs. $^{206}Pb/^{204}Pb$, **b** $^{208}Pb/^{204}Pb$ vs. $^{206}Pb/^{204}Pb$, and **c** $^{208}Pb/^{207}Pb$ vs. $^{206}Pb/^{207}Pb$. Urban aerosols from cities in Eastern China (purple triangles) from left to right in each panel are: Beijing, Hong Kong, Cheng Du, and Xin Shao[42]. The Cluster 1 ice core samples are shown for comparison as gray solid circles.

between the Pb isotope ratios of Chinese fuels with Chinese coals, they are significantly different ($p < 0.001$) and, therefore, the estimates from MixSIAR are likely accurate for fuels. Two changepoints were identified in the fuel contributions curve: one in 1974 when fuel contributions increased to ~25%, and a second changepoint in 2004 when contributions increased again after a short decrease in 2002 (Fig. 7). These findings suggest that the primary source of anthropogenic Pb at Guliya was derived from gasoline combustion.

Regarding the contribution of natural sources, since the Pb isotope ratios of Chinese coal overlap with the Pb isotopic fingerprint of the TP PSA, natural contribution estimates are probably underestimated. Thus, we suggest that both the TP and the Taklamakan PSAs are the most likely primary natural sources accounting for 70% of the Pb before 1974 and decreasing to ~50% and 35% of the Pb in 1974 and 2000, respectively. Contributions from the Southwest Tibetan Plateau, although generally low, doubled from 10% to ~20% between 1757 and 1932 coinciding with the changepoints detected in the Pb isotope ratios (Supplementary Fig. S1) around the same years explaining the change to slightly more radiogenic Pb isotope ratios.

### Emission sources during the Industrial Revolution Period (1750–1930s)

A binomial filter applied to the Pb isotope ratios data reveals two bumps during the Industrial Revolution Period between ~1750 and ~1935. Interestingly, this is the period where sporadic (1750–1900) and consistent (1900–1930) enrichments of Pb, Sn, Cd, Zn, and Sb were previously detected[22]. The TE enrichments observed suggested a change in sources which was attributed to coal emissions from Europe at the time[22]. Although only 15 representative samples covering the 1750–1930 period were analyzed for this study, several of these samples show higher Pb isotope ratios pointing toward a change in natural sources rather than anthropogenic sources as the cause of the increased Pb EF. While the Pb isotopes provide information only about the sources of Pb, it is likely that a shift in natural

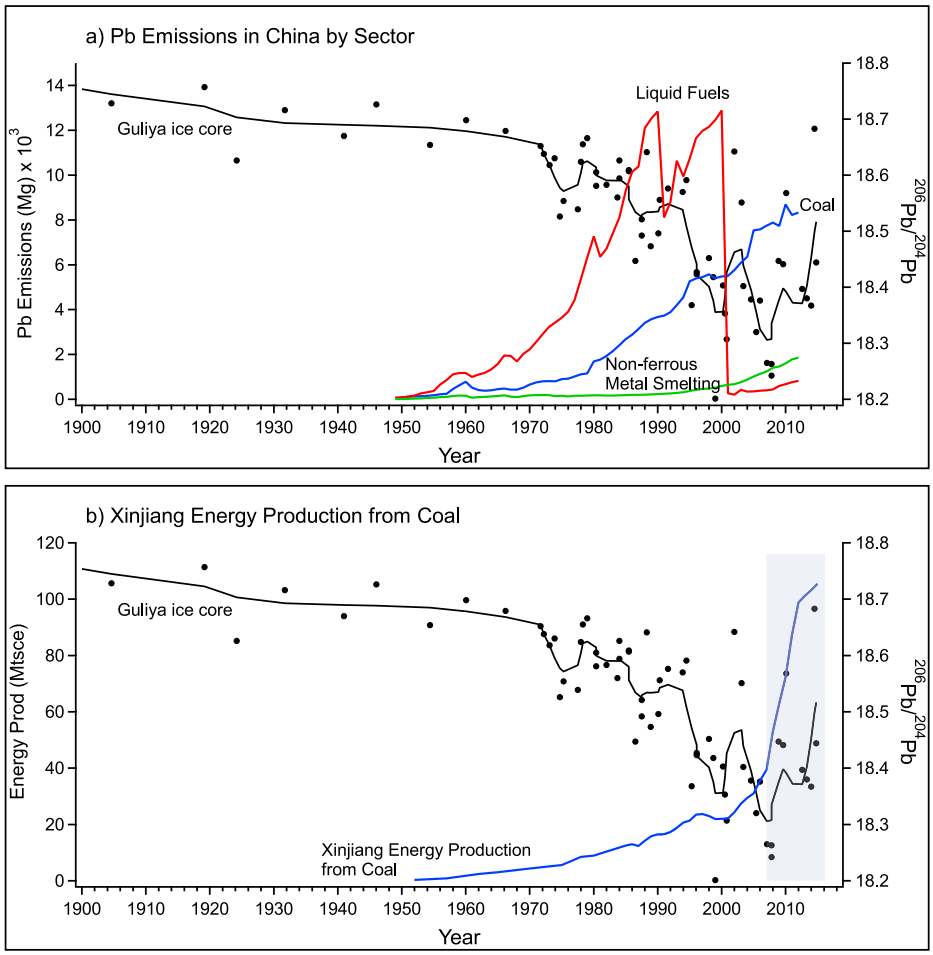


**Fig. 6 | Temporal comparisons of the $^{206}Pb/^{204}Pb$ ratios of the Guliya ice core samples with anthropogenic sources. a** Atmospheric emissions of Pb from the three primary anthropogenic sources in China between 1949 and 2012 including liquid fuels (gasoline and diesel), coal, and non-ferrous metal smelting[19], and **b** the energy produced in Xinjiang from coal combustion[64]. The solid black line represents a binomially smoothed $^{206}Pb/^{204}Pb$ isotope ratio through time. The filled light blue area in panel **b** shows the 2007–2015 period when coal combustion increased exponentially in Xinjiang.

sources also contributed to the observed enrichments of the other TEs during the same period. The Pb isotope ratios of British/European coals (Fig. 5c) are slightly lower than the TP PSA and the Cluster 1 Pb isotope ratio mean, which suggests that this was not a source of Pb during this period.

A binomial filter was also applied to the Mt. Everest data and compared with Guliya (Fig. 3). Contrary to Guliya, the Everest Pb isotope ratios decrease between 1850 and 1900 after which they increase slightly before decreasing again after ~1970. A similar antiphase effect was observed for snow accumulation during that same period for Guliya and another Himalayan ice core from the Dasuopu glacier[46]. This would support, despite the lack of a continuous record between 1850 and 1950, the likelihood that the Pb isotope ratio changes observed at Guliya and Everest might be real and that they could reflect changes in the regional atmospheric circulation.

In conclusion, the Guliya Pb isotope ice core record reveals two significant changes in Pb sources over the last 500 years. First, possible changes in atmospheric circulation between ~1750 and 1935 led to incursions of mineral dust containing Pb, likely originating from southwestern Tibet. Second, local emissions, mostly from Chinese gasoline combustion, introduced an anthropogenic signal in the Guliya Pb record starting in 1974, followed by contributions primarily from local Chinese coal combustion in 2007. The addition of the $^{204}Pb$ isotope in our isotope ratio measurements, as well as use of the Bayesian model MixSIAR, allowed us to better, and more sensitively, quantify the sources of natural and anthropogenic Pb delivered to this remote region of the world.

## Materials and methods

### The Guliya ice cores

The ice core samples used in this study originate from the Guliya ice cap (35° 17' N; 81°29' E)[23,24] in the western Kunlun Mountains at the southern border of the Xinjiang Uygur Autonomous Region in northwestern China (Fig. 1). The Guliya ice cap plateau was drilled in 1992 (GP1992) at 6200 m a.s.l[23]. and again in 2015 (GP2015). In addition, in 2015 three ice cores were extracted from the Guliya summit (GS2015) at 6700 m a.s.l.[24]. The timescale for the 1992 Guliya ice core samples was based on annual dust layer counting and was constrained to the year 1963 at 5.4 m depth where the highest beta radioactivity occurred most likely corresponding to the atmospheric thermonuclear tests performed by the former Soviet Union. The timescale for the last 1000 years of the 2015 ice core samples was developed also using annual layer counting and by constraining three reference horizons: 2015 at the surface of the glacier, 1992 at 6 m corresponding to the surface of the 1992 ice core, and 1963 at 10.9 m where the beta radioactivity rose above background levels. The timescale for the entire Holocene of the 2015 ice cores was developed using radiocarbon dating ($^{14}C$) of plant fragments found in both GP and GS cores, and with the isotopic composition of $O_2$ trapped in air bubbles in the GS cores[47]. The timescale before 15 ka BP was reconstructed using cosmogenic $^{10}Be$ and $^{36}Cl$ isotopes. Two peaks were detected in both isotopes at ~187 and ~179 m depth corresponding to the Laschamp (fixed at ~41 ka BP) and Mono Lake (fixed at ~33 ka BP) Events. A 3$^{rd}$ order polynomial was used to construct the time scale between 15 ka BP to 41 ka BP using the two cosmogenic isotope peaks. For more details the reader is referred to Thompson et al.[48].

**Ice core samples**. For this study, we used frozen archived samples that were previously processed and that had been analyzed for trace elements (TEs)[21,22]. The preparation of the ice core samples was described in detail in Sierra-Hernández et al.[21,22]. Briefly, ice core samples were cut from the corresponding ice cores in a cold room at −5 °C. Ice core samples were subsequently decontaminated in a Class 100 clean room by triple rinsing with ultrapure water at the Byrd Polar and Climate Research Center (BPCRC) at The Ohio State University (OSU). The samples were melted

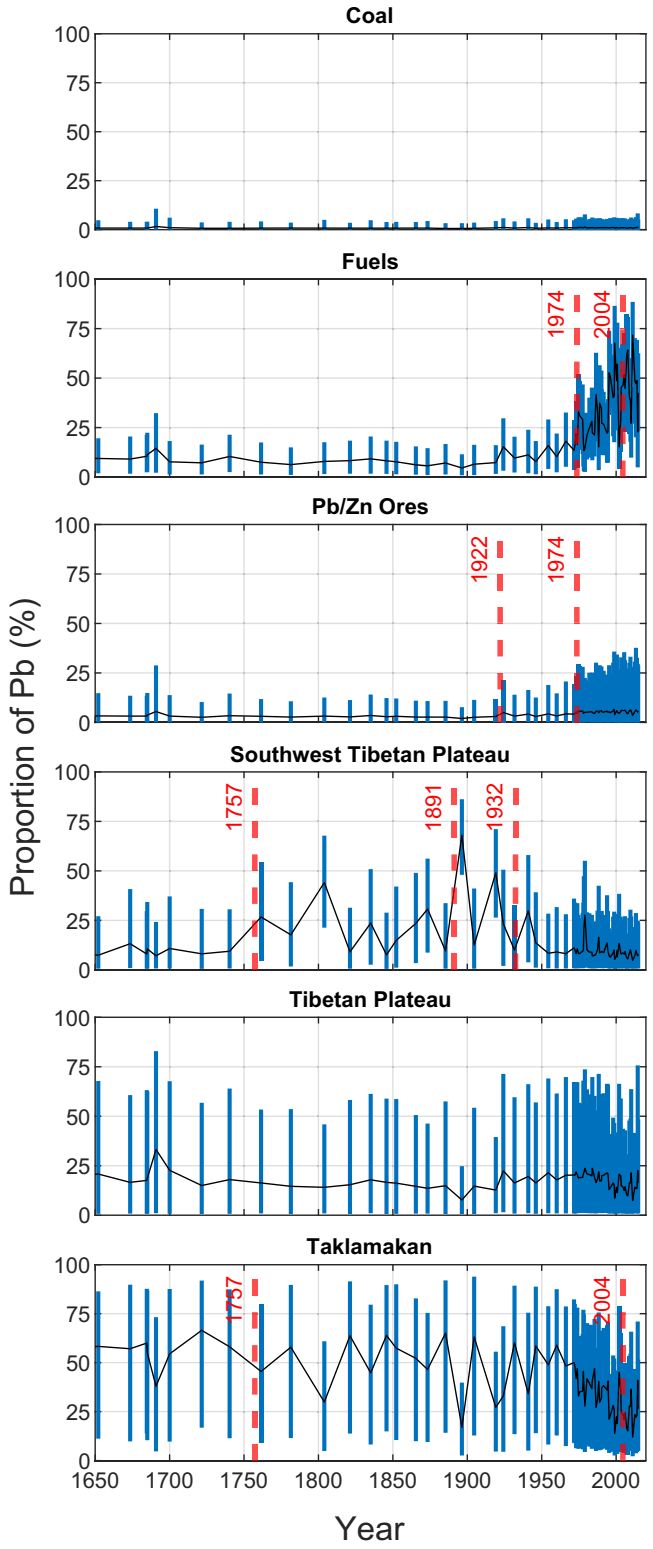


**Fig. 7 | Proportions of Pb attributed to Chinese anthropogenic sources and local PSAs calculated using the MixSIAR mixing model.** Each blue box represents the lower (2.5%) and upper (97.5%) credible intervals. The black lines represent the mean proportion for each source (means sum to 100%) and the red dashed lines the changepoints detected.

at room temperature in acid pre-cleaned low-density polyethylene (LDPE) bottles (Nalgene) and transferred to acid pre-cleaned LDPE vials. Samples were acidified to a final concentration of $HNO_3$ (Optima grade) 2% (v/v) to dissolve TEs in microparticles and to keep in solution those already dissolved. The acidified samples were kept in a class 100 clean room for 30 days to allow the acid to leach the TEs. Samples were then frozen until analysis for TEs. After the TE analysis, all samples were frozen and kept at −32 °C in the freezers at the BPCRC. The samples for this study were selected and shipped overnight to the Texas A&M University where they were kept in a freezer until analysis. The frozen archived samples were melted at room temperature before their Pb isotopic analysis.

Samples were selected to cover different periods of interest: pre-Industrial (1500-1780), Industrial (1780–1990s), and the 21st Century. Additionally, samples were selected to represent the main trends of the Pb high-resolution TE record previously observed[21,22].

A total of 89 discrete ice core samples were analyzed: 37 from GP1992 covering the period 1500–1990, 46 from GP2015 covering 1970–2015, four from GP2015 corresponding to ~36–12 ka BP, and two from GS2015 (~13.4 ka and ~3 ka BP[47]). These older samples will help establish a background prior to the Bronze Age, when metals began to be used by ancient civilizations.

**Sample selection**. The samples were selected as follows for each period of interest:

Prehistoric period prior to the Bronze Age (~36-12 ka BP): Four discrete samples from the deeper sections of the GP2015 and two samples from the deep sections of GS2015 were selected. Samples with variable dust content were selected and their ages range between 35.34 and 12.7 ka BP (1950 CE) for GP2015 and 13.35–3.5 ka BP for GS2015[47,48]. Their Pb concentrations varied between 310 to 1360 pg/g Pb.

Pre-Industrial (1500–1780): Samples were selected at ~20 years resolution to establish a pre-Industrial background. Samples with enough volume for the analysis were chosen ensuring they covered equidistant years during this period. We included samples from the three periods of Pb enrichment in Guliya during this period, 1675–1680, 1775, and 1800.

Industrial (1780–1990s): For this period samples were selected at a higher resolution (5-year resolution) than the pre-Industrial period since this period corresponds to the highest Pb enrichment observed during the 20th century.

20th and 21st Century (1971–2015): 56 samples including 21 samples from the 21st century were selected at annual and sub-annual resolutions as this is the period of main interest to understand the current changes during the 21st century for this study. Samples of low (below the median dust concentration) and high (above the median dust concentration) dust concentration were selected to determine if Pb sources changed during dust storms.

**Tibetan Plateau Potential Source Areas (PSAs)**. Pb isotopic compositions were determined for 17 dust potential source area (PSA) samples collected in the TP, including 8 sites around Guliya (TE profiles published in Sierra-Hernández et al.[22]. PSA samples were collected during different ice core field expeditions therefore they are constrained to the places visited during the respective expedition and typically named after the glacier drilled (e.g., NMY PSAs were collected during the field expedition to drill the Naimona'nyi glacier[49]). Like the ice core samples, PSA samples were prepared and analyzed previously for TEs[22,50] and were kept frozen after their TE analyses. PSA groups were formed here to facilitate source identification (see below Regional PSA Assignments).

**Analysis of Pb isotopes**. Lead isotopes ($^{204}Pb$, $^{206}Pb$, $^{207}Pb$ and $^{208}Pb$) were measured in the Radiogenic Isotope Geosciences Facility at Texas A&M University using a Thermo Scientific Neptune Plus™ High Resolution MC-ICPMS. The benefit of having the ability to measure the 204 stable isotope of Pb (which is not common in the Pb literature on ice cores analyzed to date) is that these additional data allow further identification of slight differences in sources. Excellent in-run precisions (2 s) were obtained for the $^{206}Pb/^{204}Pb$, $^{207}Pb/^{204}Pb$, and $^{208}Pb/^{204}Pb$ ratios (ranging from 0.002% to 0.4%, median of 0.01%). In-run precisions for

the ratios of the higher-abundance isotope ratios (i.e., $^{206}Pb/^{207}Pb$ and $^{206}Pb/^{208}Pb$) were better and averaged about 0.002% for all samples analyzed, irrespective of the concentrations. All samples were spiked with thallium (Tl has two stable isotopes, $^{203}Tl$ and $^{205}Tl$) to an approximate final concentration of 1 ppb and then centrifuged at 4000 rpm for 5 min before isotopic analysis. The instrumental mass fractionation of the Pb isotopes was assumed to follow that of the stable Tl isotopes[51]. Samples were aspirated directly into an APEX Omega™ desolvating nebulizer and produced Faraday cup signals of about ~500 V/ppm on the $^{208}Pb$ isotope. This amounted to about a 15 mV Faraday cup signal on $^{204}Pb$ for 1 $\times 10^3$ pg/g of total Pb. Measurements of the NBS 981 Pb isotope standard allowed additional corrections to the sample data using a bracketing technique of 3 samples to 1 standard. Corrections, assuming accurate NBS 981 Pb isotope values of 16.9406, 15.4957, and 36.7184 for the $^{206}Pb/^{204}Pb$, $^{207}Pb/^{204}Pb$, and $^{208}Pb/^{204}Pb$, respectively[52], were applied and amounted to 0.02%/amu consistently throughout the study. Duplicate analyses were performed for 7 different samples of different periods. Six blanks, prepared along with the ice core samples, were analyzed and each were found to be lower than 1 pg/g of $^{208}Pb$, making blank corrections unnecessary.

### Data analysis

A MATLAB[53] script was written to extract the samples' mean and error from the MC-ICPMS raw files to calculate the sample fractionation factors and to correct the Pb isotope ratios. Sample fractionation factors were calculated through linear interpolation using the date and analysis time of the corresponding bracketing standards.

### Enrichment factor in the Guliya ice cores

The enrichment factor (EF) is a commonly employed measure to quantify the degree to which the concentration of a specific TE has deviated from its natural background. The Guliya EFs were previously calculated[21,22] with the equation:

$$EF = [TE/Fe]_{ice}/[TE/Fe]_{PSA}$$

where $([TE]/[Fe])_{ice}$ is the TE mass ratio in the ice sample using Fe as a crustal element, while $([TE]/[Fe])_{PSA}$ is the corresponding ratio in dust samples collected close to the Guliya ice cap and used as potential source area (PSA). In the Guliya ice core, EF increases from non-crustal sources are particularly small for the Guliya ice core samples due to the high dust concentrations in the Guliya ice and to the use of local PSAs as a reference. Briefly, we note here that the absolute value of an EF depends on two factors, the crustal trace element used as a reference (Fe was used for Guliya) and on the crustal reference used. Most studies use the upper continental crust (UCC) as crustal reference while local PSA was used as reference for Guliya. The local PSA dust samples for the Guliya study were prepared (2% $HNO_3$ acidification for 30 d) and analyzed for TEs by ICP-SFMS exactly like the ice core samples. Using the same acidification method ensures that the fraction of each TE released is comparable between ice core samples and PSA. Also, using the same analytical technique and instrument greatly reduces analytical uncertainties. Also, the geochemical composition of the Guliya PSA is a much closer representation of the crustal background in the ice core samples compared to those calculated with the UCC background. It is also important to note that in addition to Fe, EFs were calculated using Al, Ba, and Mg. These EFs showed no difference compared with the EFs relative to Fe. As EF is not central in this new study, it is not discussed in more detail here. The reader is referred to the previous publications for a more in-depth discussion of the EF in the Guliya ice cores[21,22].

**Cluster analysis of samples**. To help in the determination of the sources of Pb, an unsupervised machine learning algorithm, k-means clustering analysis, was performed for both the Guliya and the PSA samples using MATLAB[54]. First, a k-means cluster analysis was performed using all normalized Pb isotope ratios ($^{206}Pb/^{204}Pb$, $^{207}Pb/^{204}Pb$, $^{208}Pb/^{204}Pb$, $^{208}Pb/^{206}Pb$, $^{206}Pb/^{207}Pb$, $^{208}Pb/^{207}Pb$), Pb concentration, and Pb EF. The Calinski-Harabasz and silhouette criteria were used to determine the optimum number of clusters. Subsequently, the Chi-square test was used to select the features that have significant associations with the obtained cluster labels. It was found that $^{206}Pb/^{204}Pb$, $^{208}Pb/^{204}Pb$, $^{208}Pb/^{206}Pb$, $^{206}Pb/^{207}Pb$, and $^{208}Pb/^{207}Pb$ were the most relevant features. A subsequent k-means cluster analysis was performed using only those five relevant Pb isotope ratios. The new cluster indices assigned were identical to those obtained from the initial analysis which indicates that the cluster classification analysis depends only on those five Pb isotope ratios.

**Three-isotope plots**. Three-isotope plots were constructed in R to compare the Guliya ice core samples with potential natural and anthropogenic sources. To facilitate this visual comparison the 17 PSAs analyzed in this study along with published PSAs from the Aral Sea[55], Taklamakan Desert[56,57], Qaidam Basin, Badain Jaran, Tengger Desert, Hongyuan, Thar Desert and the Loess Plateau[57], and Gobi Desert[58] were grouped following the k-means clustering analysis and based on their geographical origin (Supplementary Tables S1 and S2).

**MixSIAR**. The Bayesian mixing model MixSIAR developed as an open-source R package[59], is used here to quantify the contributions of Pb from the different sources as explained in the Results and Discussion section. To determine if MixSIAR is an adequate model for our study, following Longman et al.[44] univariate normality tests were performed for all sources using the Shapiro-Wilk test in RStudio and the Kolmogorov-Smirnov test in MATLAB 2023b for each $^{204}Pb$ ratio. The multivariate normal (MVN) test was applied to the three $^{204}Pb$-ratio system ($^{206}Pb/^{204}Pb$, $^{207}Pb/^{204}Pb$, and $^{208}Pb/^{204}Pb$ isotope ratios), using the package "MVN" in R. Using a $^{204}Pb$-ratio system provides maximum variability in the isotopic signature during the modeling. Additionally, having the three $^{204}Pb$ isotope ratios provides some independence among the three ratios as each Pb isotope originate from a different decay chain[44]. The model was set to "very long" Markov Chain Monte Carlo runs. A mixing polygon simulation for 3 isotopes was performed before running the mixing model to evaluate if each sample could be explained by that model using the MATLAB script developed by Smith et al.[60] (Supplementary Text S1 and Supplementary Fig. S7).

**Other statistical tests**. Additionally, the non-parametric Wilcoxon rank-sum test for two populations, means, medians, standard deviations (st dev), and changepoint detection was performed with MATLAB 2023a and 2023b. For the changepoint detection analyses, a binomial filter was first applied to smooth the datasets. The smoothed datasets were converted into regularly spaced datasets of 200 points using linear interpolation, after which changepoint detection was applied to the processed data using the mean statistic (Fig. 7, Supplementary Fig. S1).

**Regional PSA assignments**. The Pb isotopic ratios of the 17 PSA samples are shown in Table 2. The most noticeable feature is that PSAs are more radiogenic (i.e., higher isotope ratio values) towards the southern part of the TP (NMY 8, NMY 9, and NMY 21 collected around the Himalayas, Supplementary Fig. S5) with mean $^{206}Pb/^{204}Pb$, $^{207}Pb/^{204}Pb$, and $^{208}Pb/^{204}Pb$ ratios of 18.900, 15.753, and 39.357, respectively. These ratios are similar to those found in soil samples from Ngari in the southern TP[61]. Huahaizi, the most northern PSA is the least radiogenic of our PSA samples with mean $^{206}Pb/^{204}Pb$, $^{207}Pb/^{204}Pb$, and $^{208}Pb/^{204}Pb$ isotope ratios of 18.473, 15.645, and 38.730, respectively. In another study, Pb isotope ratios in soil samples from Hongyuan, southeast of Huahizi, were determined to be 18.756, 15.683, and 39.045 for $^{206}Pb/^{204}Pb$, $^{207}Pb/^{204}Pb$, and $^{208}Pb/^{204}Pb$, respectively[57]. This north-south Pb gradient extends beyond the TP PSA samples measured here. The Gobi Desert, the most northern desert considered in this study has the lowest $^{206}Pb/^{204}Pb$, $^{207}Pb/^{204}Pb$, and $^{208}Pb/^{204}Pb$ isotope ratios, 18.841, 15.638, and 38.641, respectively[58], while the same ratios in the Thar desert

in northwestern India are the most radiogenic (18.657, 15.857, and 40.009, respectively[57]). This gradient is clearly apparent in a map of $^{208}Pb/^{204}Pb$ isotope ratios for our and published PSAs used in this study (Supplementary Fig. S5). This latitudinal gradient was also observed in snow pit samples from glaciers in western China with snow samples being more radiogenic in the south compared to the north[62], further confirming the north-south radiogenic gradient observed in our PSAs.

The k-means clustering analysis grouped all PSAs, both from previous publications and this study, into three clusters (Supplementary Table S1). Two of these clusters (Clusters 2 and 3 in Supplementary Table S1) comprised PSAs that are similar to each other in their respective cluster. The rest of the PSAs (Cluster 1) seemed to have clustered together because of their dissimilarity with those in Clusters 2 and 3 as described below.

Cluster 1 is formed mostly by a group of PSAs from different deserts and regions that are distinct from those in Cluster 2. The PSAs of Cluster 1 are mostly outside of the TP (Taklamakan Desert, Loess Plateau, Gobi Desert) or at the margins of the TP (Hongyuan in the far eastern TP, and some of the NMY PSAs from the Himalayas), and Cluster 1 includes the two PSAs collected by lakes during the Guliya 2015 field expedition. These two lake PSAs seem quite different than the rest of PSAs collected around Guliya, perhaps because of the influence of the lake sediments which would explain why they were grouped in Cluster 1. The Pb isotope ratios of Cluster 1 show high variability likely because they originate from different regions with distinct Pb isotopic fingerprints. The means and standard deviations of Cluster 1 are 18.832 and 0.065 for $^{208}Pb/^{204}Pb$; 15.684 and 0.037 for $^{207}Pb/^{204}Pb$; and 38.996 and 0.210 for $^{208}Pb/^{204}Pb$.

Cluster 2 is comprised mostly of PSAs with low Pb isotopic variability with means and standard deviations of 18.628 and 0.063 for $^{208}Pb/^{204}Pb$; 15.655 and 0.017 for $^{207}Pb/^{204}Pb$; and 38.864 and 0.120 for $^{208}Pb/^{204}Pb$. PSAs in Cluster 2 are from the main TP and from northeastern TP including the Qaidam Basin, Badain Jaran Desert and Tengger Desert, and NMY 3 from the Himalayas. Interestingly one sample from the far north edge of the Taklamakan desert[57,63] was grouped in this Cluster 2. The northern edge of the Taklamakan desert borders the Tian Shan mountains, which while not within the TP, form part of the mountainous region within the Pamir and the Kunlun Mountains where Guliya is located in northwestern Tibet. For the analysis of potential sources in this study, even though PSAs were grouped in this Cluster 2, we split them into different PSA groups according to their geographical region as shown in Tables 2 and 3 to keep sources upwind and west of Guliya separated from those downwind and east of Guliya.

Cluster 3 comprises exclusively the PSAs from the Thar Desert which are noticeably different from any of the other PSAs with the highest $^{207}Pb/^{204}Pb$ and $^{208}Pb/^{204}Pb$ isotope ratios in the region.

## Data availability

The authors declare that the data supporting the findings of this study are available within the paper and its supplementary information files. The Pb isotope ratios of the ice core samples are archived at https://www.ncei.noaa.gov/access/paleo-search/study/39780 from the NOAA National Centers for Environmental Information.

## Code availability

The codes used in this study are accessible upon request from the corresponding author.

Received: 12 March 2024; Accepted: 24 September 2024;
Published online: 01 October 2024

## References

1. Gerhardsson, L., Lead, in Elements and their Compounds in the Environment. In *Occurrence, Analysis and Biological Relevance* (eds, Merian, E. et al.) 879–900 (WILEY-VCH, 2004).
2. Koller, K. et al. Recent Developments in Low-Level Lead Exposure and Intellectual Impairment in Children. *Environ. Health Perspect.* **112**, 987–994 (2004).
3. Lanphear, B. P. et al. Low-level lead exposure and mortality in US adults: a population-based cohort study. *Lancet Public Health* **3**, e177–e184 (2018).
4. Poręba, R. et al. Environmental and occupational exposure to lead as a potential risk factor for cardiovascular disease. *Environ. Toxicol. Pharmacol.* **31**, 267–277 (2011).
5. Rocha, A. & Trujillo, K. A. Neurotoxicity of low-level lead exposure: History, mechanisms of action, and behavioral effects in humans and preclinical models. *NeuroToxicology* **73**, 58–80 (2019).
6. Spivey, A. The weight of lead. Effects add up in adults. *Environ. Health Perspect.* **115**, A30–A36 (2007).
7. Nriagu, J. O., *Lead and Lead Poisoning in Antiquity*, 437 (John Wiley & Sons, 1983).
8. Wertime, T. A. The Beginnings of Metallurgy: A New Look. *Science* **182**, 875 (1973).
9. Yahalom-Mack, N. et al. The Earliest Lead Object in the Levant. *PLOS One* **10**, e0142948 (2015).
10. Liu, R., Rawson, J. & Pollard, A. M. Beyond ritual bronzes: identifying multiple sources of highly radiogenic lead across Chinese history. *Sci. Rep.* **8**, 11770 (2018).
11. Meicun, L. & Liu, X. The origins of metallurgy in China. *Antiquity* **91**, e6 (2017).
12. Schafer, E. H. The Early History of Lead Pigments and Cosmetics in China. *T'oung Pao* **44**, 413–438 (1956).
13. Sun, W. D. et al. Origin of the mysterious Yin-Shang bronzes in China indicated by lead isotopes. *Sci. Rep.* **6**, 23304 (2016).
14. Nriagu, J. O., Natural Versus Anthropogenic Emissions of Trace Metals to the Atmosphere. In *Control and Fate of Atmospheric Trace Metals* (eds, Pacyna, J. & Ottar, B.) 3–13 (Kluwer Academic Publishers, 1989).
15. Nriagu, J. O. & Pacyna, J. M. Quantitative assessment of worldwide contamination of air, water and soils by trace metals. *Nature* **333**, 134–139 (1988).
16. Javed, M. B. et al. Size-resolved Pb distribution in the Athabasca River shows snowmelt in the bituminous sands region an insignificant source of dissolved Pb. *Sci. Rep.* **7**, 43622 (2017).
17. Marx, S. K., Rashid, S. & Stromsoe, N. Global-scale patterns in anthropogenic Pb contamination reconstructed from natural archives. *Environ. Pollut.* **213**, 283–298 (2016).
18. Pacyna, J. M., Pacyna, E. G. & Aas, W. Changes of emissions and atmospheric deposition of mercury, lead, and cadmium. *Atmos. Environ.* **43**, 117–127 (2009).
19. Tian, H. Z. et al. Quantitative assessment of atmospheric emissions of toxic heavy metals from anthropogenic sources in China: historical trend, spatial distribution, uncertainties, and control policies. *Atmos. Chem. Phys.* **15**, 10127–10147 (2015).
20. Wan, D. et al. Spatiotemporal trends of atmospheric Pb over the last century across inland China. *Sci. Total Environ.* **729**, 138399 (2020).
21. Sierra-Hernández, M. R. et al. 21st-century Asian air pollution impacts glacier in northwestern Tibet. *Atmos. Chem. Phys.* **19**, 15533–15544 (2019).
22. Sierra-Hernández, M. R. et al. Atmospheric depositions of natural and anthropogenic trace elements on the Guliya ice cap (northwestern Tibetan Plateau) during the last 340 years. *Atmos. Environ.* **176**, 91–102 (2018).
23. Thompson, L. G. et al. A 1000 year ice core climate record from the Guliya Ice Cap, China and its relationship to global climate variability. *Ann. Glaciol.* **21**, 175–181 (1995).
24. Thompson, L. G. et al. Ice core records of climate variability on the Third Pole with emphasis on the Guliya ice cap, western Kunlun Mountains. *Quat. Sci. Rev.* **188**, 1–14 (2018).
25. Wang, W., et al. Assessing Sources and Distribution of Heavy Metals in Environmental Media of the Tibetan Plateau: A Critical Review. *Front. Environ. Sci.* **10**, 874635 (2022).

26. Li, Q. et al. The estimated atmospheric lead emissions in China, 1990–2009. *Atmos. Environ.* **60**, 1–8 (2012).
27. Pompeani, D. P. et al. Lake Sediments Record Prehistoric Lead Pollution Related to Early Copper Production in North America. *Environ. Sci. Technol.* **47**, 5545–5552 (2013).
28. Lee, C. S. L. et al. Seven Thousand Years of Records on the Mining and Utilization of Metals from Lake Sediments in Central China. *Environ. Sci. Technol.* **42**, 4732–4738 (2008).
29. Lee, K. et al. Isotopic signatures for natural versus anthropogenic Pb in high-altitude Mt. Everest ice cores during the past 800 years. *Sci. Total Environ.* **412**, 194–202 (2011).
30. Osterberg, E. et al. Ice core record of rising lead pollution in the North Pacific atmosphere. *Geophys. Res. Lett.* **35**, L05810 (2008).
31. Harlavan, Y. & Erel, Y. The release of Pb and REE from granitoids by the dissolution of accessory phases. *Geochim. Cosmochim. Acta* **66**, 837–848 (2002).
32. Bing, H. et al. Historical trends of anthropogenic metals in Eastern Tibetan Plateau as reconstructed from alpine lake sediments over the last century. *Chemosphere* **148**, 211–219 (2016).
33. Bao, K. et al. Atmospheric Deposition History of Trace Metals and Metalloids for the Last 200 Years Recorded by Three Peat Cores in Great Hinggan Mountain, Northeast China. *Atmosphere* **6**, 380–409 (2015).
34. Eichler, A. et al. Three Centuries of Eastern European and Altai Lead Emissions Recorded in a Belukha Ice Core. *Environ. Sci. Technol.* **46**, 4323–4330 (2012).
35. Wensman, S. M., Shiel, A. E. & McConnell, J. R. Lead isotopic fingerprinting of 250-years of industrial era pollution in Greenland ice. *Anthropocene* **38**, 100340 (2022).
36. Schwikowski, M. et al. Post-17th-Century Changes of European Lead Emissions Recorded in High-Altitude Alpine Snow and Ice. *Environ. Sci. Technol.* **38**, 957–964 (2004).
37. Bi, X.-Y. et al. Lead Isotopic Compositions of Selected Coals, Pb/Zn Ores and Fuels in China and the Application for Source Tracing. *Environ. Sci. Technol.* **51**, 13502–13508 (2017).
38. Chiaradia, M. & Cupelin, F. Behaviour of airborne lead and temporal variations of its source effects in Geneva (Switzerland): comparison of anthropogenic versus natural processes. *Atmos. Environ.* **34**, 959–971 (2000).
39. Farmer, J. G., Eades, L. J. & Graham, M. C. The lead content and isotopic composition of british coals and their implications for past and present releases of lead to the UK environment. *Environ. Geochem. Health* **21**, 257–272 (1999).
40. Monna, F. et al. Pb Isotopic Composition of Airborne Particulate Material from France and the Southern United Kingdom: Implications for Pb Pollution Sources in Urban Areas. *Environ. Sci. Technol.* **31**, 2277–2286 (1997).
41. Mukai, H. et al. Lead isotope ratios in the urban air of eastern and central Russia. *Atmos. Environ.* **35**, 2783–2793 (2001).
42. Bollhöfer, A. & Rosman, K. J. R. Isotopic source signatures for atmospheric lead: the Northern Hemisphere. *Geochim. Cosmochim. Acta* **65**, 1727–1740 (2001).
43. Dietrich, M. et al. Quantification of Pb pollution sources in complex urban environments through a multi-source isotope mixing model based on Pb isotopes in lichens and road sediment. *Environ. Pollut.* **288**, 117815 (2021).
44. Longman, J. et al. Quantitative assessment of Pb sources in isotopic mixtures using a Bayesian mixing model. *Sci. Rep.* **8**, 6154 (2018).
45. Koffman, B. G. et al. Provenance of Anthropogenic Pb and Atmospheric Dust to Northwestern North America. *Environ. Sci. Technol.* **56**, 13107–13118 (2022).
46. Thompson, L. G. et al. Abrupt Tropical Climate Change: Past and Present. *Proc. Natl Acad. Sci. USA* **103**, 10536–10543 (2006).
47. Thompson, L. G. et al. Use of δ18Oatm in dating a Tibetan ice core record of Holocene/Late Glacial climate. *Proc. Natl Acad. Sci.* **119**, e2205545119 (2022).
48. Thompson, L. G. et al. Ice core evidence for an orbital-scale climate transition on the Northwest Tibetan Plateau. *Quat. Sci. Rev.* **324**, 108443 (2024).
49. Kehrwald, N. M., et al. Mass loss on Himalayan glacier endangers water resources. *Geophys. Res. Lett.* **35**, L22503 (2008).
50. Beaudon, E. et al. Central Tibetan Plateau atmospheric trace metals contamination: A 500-year record from the Puruogangri ice core. *Sci. Total Environ.* **601**, 1349–1363 (2017).
51. Taylor, R. N. et al. Evaluating the precision of Pb isotope measurement by mass spectrometry. *J. Anal. At. Spectrom.* **30**, 198–213 (2015).
52. Yuan, H. et al. Evaluation of lead isotope compositions of NIST NBS 981 measured by thermal ionization mass spectrometer and multiple-collector inductively coupled plasma mass spectrometer. *Solid Earth Sci.* **1**, 74–78 (2016).
53. *MATLAB* (The MathWorks Inc, 2023).
54. MATLAB. *Statistics and Machine Learning Toolbox* (The MathWorks Inc., 2023).
55. Dewan, N. et al. Stable isotopes of lead and strontium as tracers of sources of airborne particulate matter in Kyrgyzstan. *Atmos. Environ.* **120**, 438–446 (2015).
56. Bory, A. J. M. et al. A Chinese Imprint in Insoluble Pollutants Recently Deposited in Central Greenland As Indicated by Lead Isotopes. *Environ. Sci. Technol.* **48**, 1451–1457 (2014).
57. Ferrat, M. et al. Lead atmospheric deposition rates and isotopic trends in Asian dust during the last 9.5kyr recorded in an ombrotrophic peat bog on the eastern Qinghai–Tibetan Plateau. *Geochim. Cosmochim. Acta* **82**, 4–22 (2012).
58. Biscaye, P. E. et al. Asian provenance of glacial dust (stage 2) in the Greenland Ice Sheet Project 2 Ice Core, Summit, Greenland. *J. Geophys. Res. Oceans* **102**, 26765–26781 (1997).
59. Stock, B. C. et al. Analyzing mixing systems using a new generation of Bayesian tracer mixing models. *PeerJ* **6**, e5096 (2018).
60. Smith, J. A. et al. To fit or not to fit: evaluating stable isotope mixing models using simulated mixing polygons. *Methods Ecol. Evol.* **4**, 612–618 (2013).
61. Du, Z. et al. Dust provenance in Pan-third pole modern glacierized regions: What is the regional source? *Environ. Pollut.* **250**, 762–772 (2019).
62. Yu, G. et al. Lead isotopic composition of insoluble particles from widespread mountain glaciers in western China: Natural vs. anthropogenic sources. *Atmos. Environ.* **75**, 224–232 (2013).
63. Ferrat, M. et al. Improved provenance tracing of Asian dust sources using rare earth elements and selected trace elements for palaeomonsoon studies on the eastern Tibetan Plateau. *Geochim. Cosmochim. Acta* **75**, 6374–6399 (2011).
64. Jianxin, J. *Xinjiang Statistical Yearbook* (China Statistics Press, 2016).


## Acknowledgements

This research was funded by the National Science Foundation, GG program of the Directorate for Geosciences grant no. EAR-2222051 to MRSH, EMG, and LGT, and EAR-2222052 to F.M. Additional financial support to F.M. was provided by the generosity of the late R. Ken and Jane Williams. The authors are grateful to everyone who made the 1992 and the 2015 Guliya field expeditions a success, in particular Tandong Yao from the Institute for Tibetan Plateau Research. Likewise, we acknowledge Natalie M. Kehrwald for collecting the NMY PSA dust samples. The authors would also like to acknowledge Dominic Woelki for his support in the lab for the MC-ICPMS analyses. M.R.S.H. is thankful to Emilie Beaudon for working with her in the preparation of the 2015 Guliya ice core samples and for valuable

discussions. M.R.S.H. thanks Hezhong Tian and Bess G. Koffman for providing Chinese Pb emissions and Jack Longman for providing his R code to run the MixSIAR model. We are also thankful to Prof. Ellen Mosley-Thompson for helping improve the English of the manuscript. M.R.S.H. is grateful to The Women's Place from The Ohio State University for providing a CD Professional Development Grant for the preliminary analysis used in the NSF proposal. This is Byrd Polar and Climate Research Center contribution no. C#1631.

## Author contributions

M.R.S.H. conceived the original idea and designed the study, performed the measurements, data analysis, and interpretation, and wrote the paper. F.M. and E.M.G. contributed to the design of the preliminary study and the conceptualization of full project. F.M. developed the analytical technique at Texas A&M for Pb isotopes, oversaw the Pb isotope analyses, ensuring the quality of both the measurements and the isotope corrections. L.G.T. led the Guliya field expedition and developed the time scale of the Guliya ice cores. All authors discussed the results and contributed to the final manuscript.

## Competing interests

The authors declare no competing interests.

## Additional information

**Supplementary information** The online version contains supplementary material available at https://doi.org/10.1038/s43247-024-01724-w.

**Correspondence** and requests for materials should be addressed to M. Roxana Sierra-Hernández.

**Peer review information** *Communications Earth & Environment* thanks Bess Koffman, Yuefang Li and the other, anonymous, reviewer(s) for their contribution to the peer review of this work. Primary Handling Editors: Yama Dixit, Aliénor Lavergne, and Carolina Ortiz Guerrero. A peer review file is available.